

## Strand Breakage Identification in Prestressed Anchorage Structures Using Stress Variation-Based Artificial Neural Networks

Ngoc-Loi Dang<sup>1)</sup>, Ngoc-Tuong-Vy Phan<sup>2)</sup>, Quoc-Bao Ta<sup>3)</sup>,  
Quang-Quang Pham<sup>4)</sup> and \*Jeong-Tae Kim<sup>5)</sup>

<sup>1),2)</sup> *Urban Infrastructure Faculty, Mien Tay Construction University, Vinh Long, Vietnam*

<sup>3),4),5)</sup> *Department of Ocean Engineering, PKNU, Busan 608-737, Korea*

<sup>\*</sup>[idis@pknu.ac.kr](mailto:idis@pknu.ac.kr)

### ABSTRACT

In this study, strand breakage identification in prestressed multi-strand anchorages using stress variation-based artificial neural networks (ANN) algorithm is investigated. Firstly, a scheme of stress variation-based ANN is designed for damage detection in the anchorage structures. The ANN architecture comprises an input, an output, and hidden layers. Variations of stress components are utilized as the input, while the output consists of prestressing loss levels of strands. Second, the FE (finite element) model of an actual multi-strand anchorage is analyzed to generate training patterns under various single and multiple damaged strand cases. Third, the ANN algorithms are trained using training patterns and employed to detect damaged strand locations and severities in the multi-strand anchorage. Last, the feasibility of trained ANN models for prestress loss estimation is tested using experimental data. The result proves that the proposed method is promising to be applied for prestress loss identification in the anchorage with relatively high predicting accuracy.

### 1. INTRODUCTION

The post-tensioning technique has been extensively used for the construction of civil infrastructures (e.g., bridges). In post-tensioning structures, prestressing force is a main parameter that can reveal the structural health conditions. Due to various operating conditions and prestressing techniques, structures are prone to instantaneous and long-term prestress losses (Tadros *et al.* 2003). Due to its critical role of prestressing force, it should be monitored to ensure structural integrity.

Various structural health monitoring methods have been developed to detect structural damage to PSC structures. Visual inspection using the unmanned aerial

---

<sup>1)</sup> PhD

<sup>2)</sup> MSc

<sup>3)4)</sup> Graduate student

<sup>5)</sup> Professor

vehicle has emerged for bridge inspection (Spencer *et al.* 2019), such as cracks and spalling on surfaces of decks and piers. Nonetheless, the technique is not suitable for detecting invisible defects (e.g., prestress loss) in inspected structures. Vibration-based methods have been developed to identify prestress force by utilizing the vibration properties of a structure, such as natural frequencies. The method was applied for prestress force estimation in cable-stayed bridges (Zui *et al.* 1996) and lab-scale model of PSC girders (Kim *et al.* 2004, Ho *et al.* 2012). However, the vibration-based methods utilize low-order modal parameters, which are insensitive to local and incipient structural damages (Law *et al.* 2005, Hamed *et al.* 2006).

Impedance-based methods have been adopted to detect the prestress-loss in post-tensioned concrete structures (Kim *et al.* 2010, Huynh *et al.* 2014, Min *et al.* 2016, Dang *et al.* 2019). It was found that impedance signatures were significantly changed in impedance features under temperature variations (Huynh *et al.* 2017), demanding high computational cost for temperature compensation effects on impedance features (Zhang *et al.* 2019). Acoustoelastic-based methods have been tested in laboratory conditions and in-situ PSC girders. Using the tested velocity on a 4.8 m long prestressing strand, it was found that the relationship between the time shift and the force levels was nonlinear when the ultimate tensile strength (UTS) of the strand was greater than 70% of UTS (Chen *et al.* 2001). Also, the measured acoustic signals of interest included noise (e.g., ambient vibrations) (Salamone *et al.* 2011), thus demanding a specialized technique for filtering the noise to be sufficient for identifying the acoustic emission of the interest.

Strain-based methods are regarded as simple and accurate techniques to estimate prestress levels by using a well-defined stress-strain relationship (Barr *et al.* 2008). Abdullah *et al.* (2015a) affixed an array of electrical strain gauges (ESGs) on a multi-strand anchor's face to detect wire breaks using measured strain variation before and after cutting steel wires. ESGs arrays were used to determine damage-sensitive sensor placement in the anchorage structure (Dang *et al.* 2020).

In prestressed multi-strand anchorage, strand breakage can occur at any strand with an unknown prestress force level. It is necessary to localize and accurately estimate prestress force loss. In this study, strand breakage identification in a prestressed anchorage using stress variation-based artificial neural networks (ANN) algorithm is investigated. Firstly, a scheme of stress variation-based ANN is designed for damage detection in the anchorage structures. The ANNs architecture comprises an input, an output, and hidden layers. Two stress variation components are utilized as the input, while the output consists of prestressing loss levels of strands. Second, the FE (finite element) model of a real multi-strand anchorage is analyzed to generate training patterns under various single and multiple damaged strand cases. Third, the ANN algorithms are trained using training patterns and employed to detect damaged strand locations and severities in the multi-strand anchorage. Last, the feasibility of trained ANN models for prestress loss estimation is tested using experimental data.

## **2. SCHEME OF STRAND BREAKAGE IDENTIFICATION**

Fig. 1 shows an overview of circumferential stress distribution in the anchorage under a strand breakage case. The anchorage consists of a bearing plate and multi-

strand anchor head. Due to prestressing strands directly anchored into the anchor head, the strand breakage mostly caused stress change in the anchor head (see Fig. 1) rather than the whole PSC structure (Abdullah *et al.* 2015b). Fig. 1c shows the attachment of an electrical strain gage (ESG) array to get strain signals in the anchorage. The ESGs should be placed at the damage-sensitive location to signify strain signals for damage detection tasks (Dang *et al.* 2020). As presented in the previous study, the near-top anchor head is more sensitive to circumferential stress change, while the near-bottom is more sensitive to axial stress variation. The stress components were selected as a training pattern for ANN models.

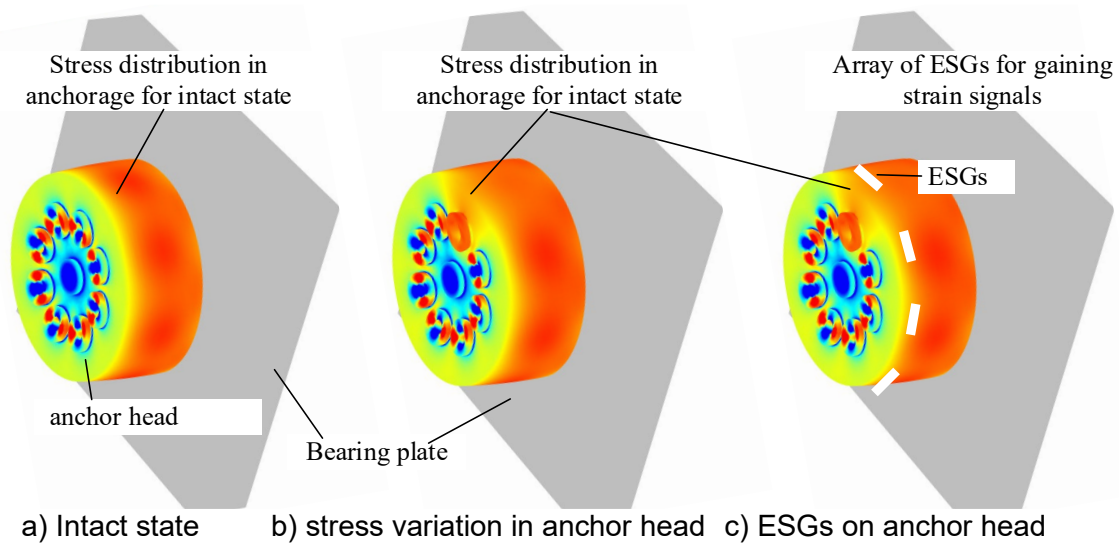


Fig. 1 Overview of circumferential stress distribution in the anchorage

Fig. 2 shows a scheme of stress variation-based ANNs for damage identification in anchorage structure. The algorithm using feed-forward neural networks consists of an input, an output, and hidden layers. The activation functions are sigmoid in the hidden layers and linear function in the output layer.

The training of stress variation-based ANNs is performed in the following steps. First, a baseline finite element model of a selected anchorage is established in commercial software. Second, single and multiple damage scenarios are selected based on the potentially damaged strands in the post-tensioning anchorage zone. Each damage scenario contains two important parameters, which are location and severity. The single damage can locate at any strand. Meanwhile, the multiple damages are assumed to be only concurrent damage of two strands. Variations of stress components after and before damage are calculated to build data bank for single and multiple damages independently. Finally, these data sets are used for training stress variation-based ANN algorithms.

Four ANNs are built for single and multiple damage detection of the multiple prestressed strands using circumferential and axial stress variations. Specifically, circumferential stress change-based ANNs for single damage detection (namely CAS), axial stress change-based ANNs for single damage detection (AAS), circumferential

stress change-based ANNs for multiple damage detection (CAM), and axial stress change-based ANNs for multiple damage detection (AAM).

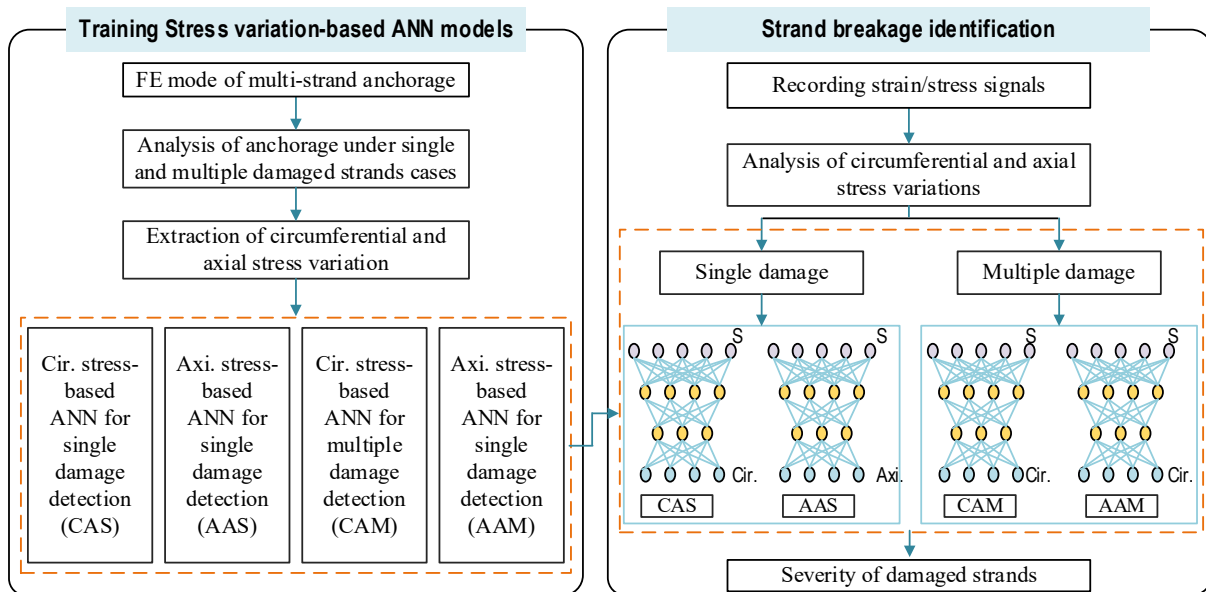


Fig. 2 Scheme of stress variation-based ANNs for damage identification

Fig. 3 shows the architecture of stress variation-based ANN models. For the circumferential stress (see Fig. 3a), the input layer is composed of the variations of circumferential stress at the near-top anchor head, which were obtained via CT1-CT8 in the measured structure. It is noted that CT1-CT8 is used to get stress variation for the single and multiple damages. A strand is randomly simulated by reducing prestressing force from 0-14 kN with an interval of 3.5 kN. Totally, there are 45 cases of simulated prestressing forces for training the CAS and AAS models separately, as seen in Table 1. There are two hidden layers, consisting of 50 neurons in each layer, were selected for each layer.

For the axial stress component (see Fig. 3b), the input layer is composed of the variations of axial stress at the near-bottom anchor head, which were obtained via AB1-AB8 in the measured structure. Two strands are randomly simulated by reducing prestressing force from 0-14 kN with an interval of 3.5 kN. Totally, there are 1600 cases of simulated prestressing forces for training the CAM and AAM models, as seen in Table 1. Two hidden layers, 50 neurons for each layer, are also used for training the CAM and AAM models.

After the training process, variations of stress component-based ANNs (i.e., CAS, AAS, CAM and AAM models) are employed to identify strand locations and their severity.

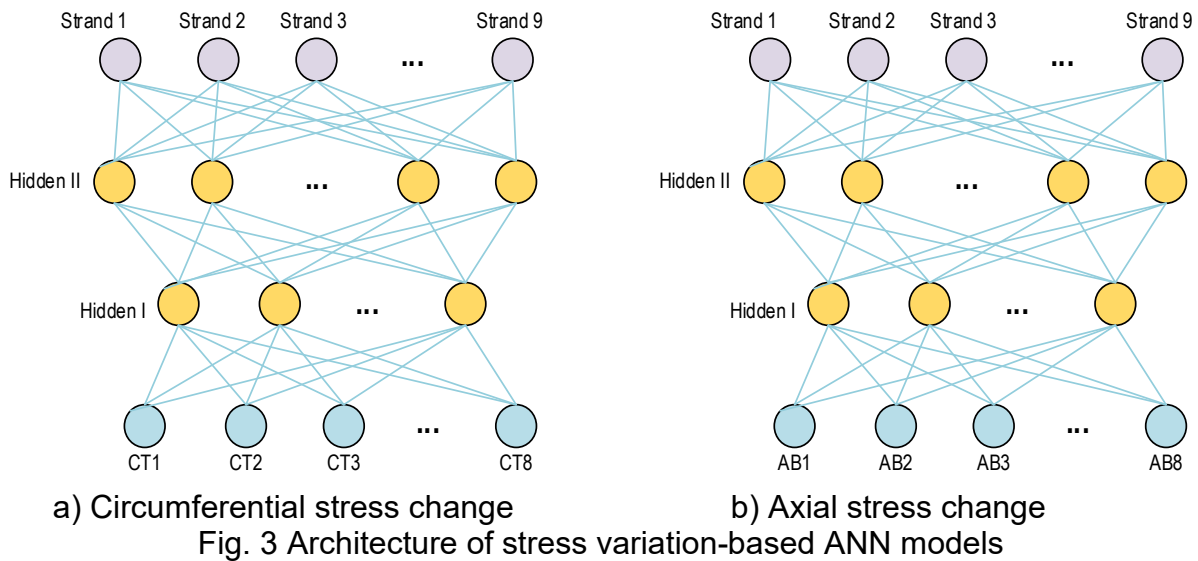


Table 1 Properties of variation of stress component-based ANNs for damage detection

| ANN properties        | Single damage for CAS and AAS models | Multiple damages for CAM and AAM models |
|-----------------------|--------------------------------------|---|
| No. Training patterns | 45                                   | 1600                                    |
| No. Input neurons     | 8                                    | 8                                       |
| No. Hidden 1 neurons  | 50                                   | 50                                      |
| No. Hidden 2 neurons  | 50                                   | 50                                      |
| No. Output neurons    | 9                                    | 9                                       |

### 3. STRESS ANALYSIS OF MULTI-STRAND ANCHORAGE

#### 3.1 FEM of Multi-strand Anchorage

To analyze the stress variation induced by local strand breakage, a finite element (FE) model of a multi-strands anchorage was established using COMSOL Multiphysics. The FE model consists of a bearing plate and 9-strand anchor head with 9-wedges, as shown in Fig. 4. The anchorage was designed to fit with seven strands 15.2 mm. The bearing plate has a size of 270×270×45 mm, the anchor head has  $\phi$ 159 mm and 70 mm in height, and the wedge has top and bottom diameters of 29 mm and 17 mm, respectively.

The FE model was meshed by three-dimensional (3D) elements. Tetrahedron elements were used to mesh the bearing plate, and the anchor head and hexahedron elements were used for the wedges. The material properties of the steel anchorage components is defined as follows:  $E = 200$  GPa (Young modulus),  $\nu = 0.33$  (Poisson ratio), and  $\rho = 7850$  kg/m<sup>3</sup> (mass density). The perfect contact conditions between the anchor head and the bearing plate were used for the contact between the wedge and the

anchor head. 3D-spring contacts (Huynh *et al.* 2015) were assigned at the bottom of the bearing plate.

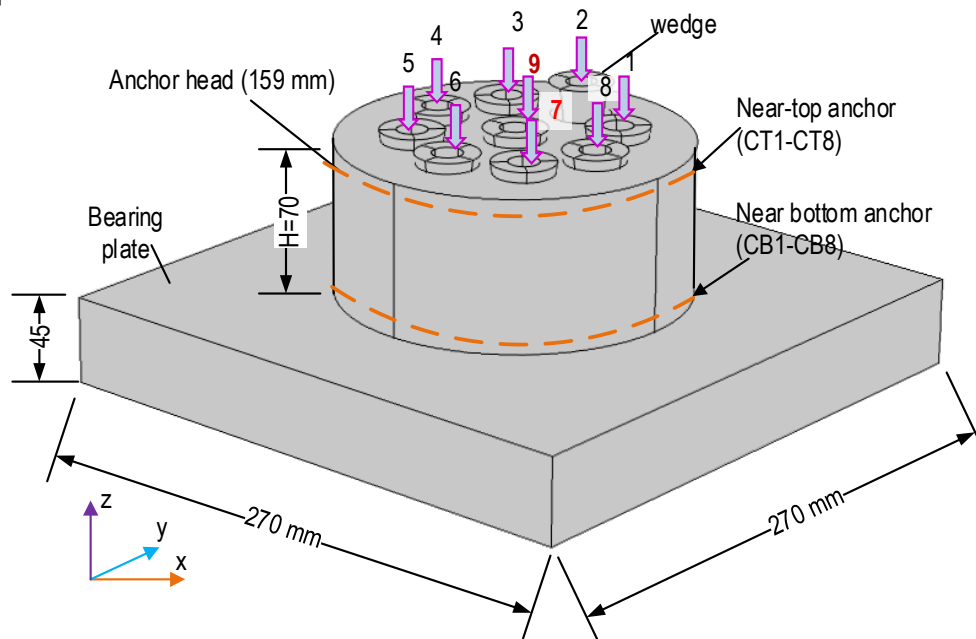


Fig. 4 FE model of 9-strands anchorage system for stress analysis

The stress analysis was performed on the FE model under the intact and strand breakage cases. In the intact case, each of the nine wedges was assigned with a force of 140 kN to simulate the prestressing forces. In damage cases, assigned forces in strands were reduced with an interval of 35 kN to simulate prestressing force losses. The total simulated cases are listed in Table 1. For each simulation case, the circumferential stress was extracted at the near-top anchor head (3 mm from wedge plate) via CT1-CT8. Each sensor location was placed uniformly on the circumference. Meanwhile, the axial stress was extracted at the near-bottom anchor head via AB1-AB8 (5 mm from the surface of the bearing plate).

### 3.2 Variation of Stress Fields due to Local Strand Breakage

Fig. 5 shows the stress field change induced by the strand breakage event in the anchorage. For the circumferential stress, the near-top anchor head experienced more stress variation than the bottom one (Fig. 5a) under an outer breakage. For the axial stress, the near-bottom anchor head experienced more stress variation than the bottom one (Fig. 5b) under an outer breakage.

Fig. 6a shows the variation of axial stress obtained from the near-bottom anchor head under 35 kN loss of Strand 1. The maximum stress change was found at the local damage strand (i.e., Strand 1), and stress change at two adjunct strands (e.g., Strand 2) was less than a haft compared with that at Strand 1. Fig. 6b shows the variation of circumferential stress obtained from the near-top anchor head under 35 kN loss of Strand 1. The maximum stress change was found at the local damaged Strand 1, while the stress change at other strands was insignificant.

Fig. 7a shows the variation of axial stress obtained from the near-bottom anchor head under 50 kN force loss of Strand 1 and 70 kN force loss of Strand 4. The maximum stress change was found at Strand 4. Meanwhile, the stress changes of Strand 1, 3, and 5 were also significant. Fig. 7b shows the variation of circumferential stress obtained from the near-top anchor head under the losses of 50 kN-Strand 1 and 70 kN-Strand 1. The first and second largest stress change was located at damaged Strand 4 and Strand 1, respectively. Moreover, the stress change at other strands was ignorable.

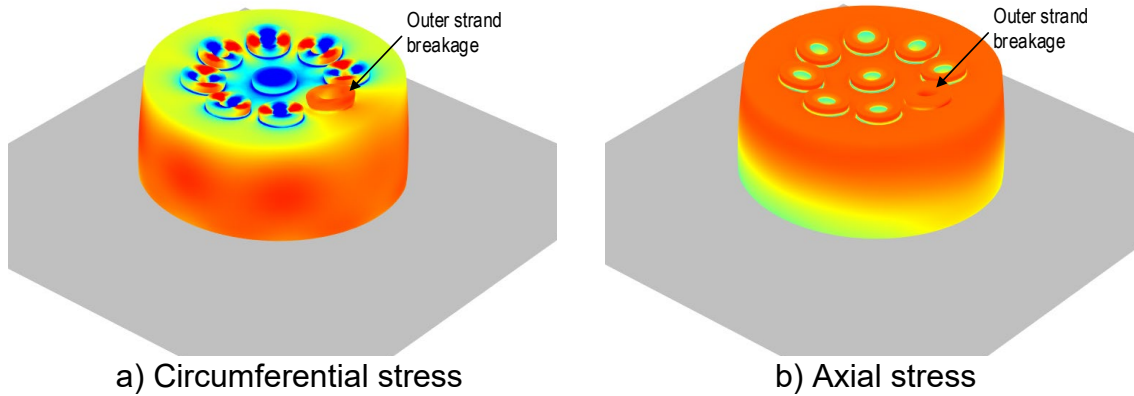


Fig. 5 Variation of stress fields in the anchor head induced by strand breakage

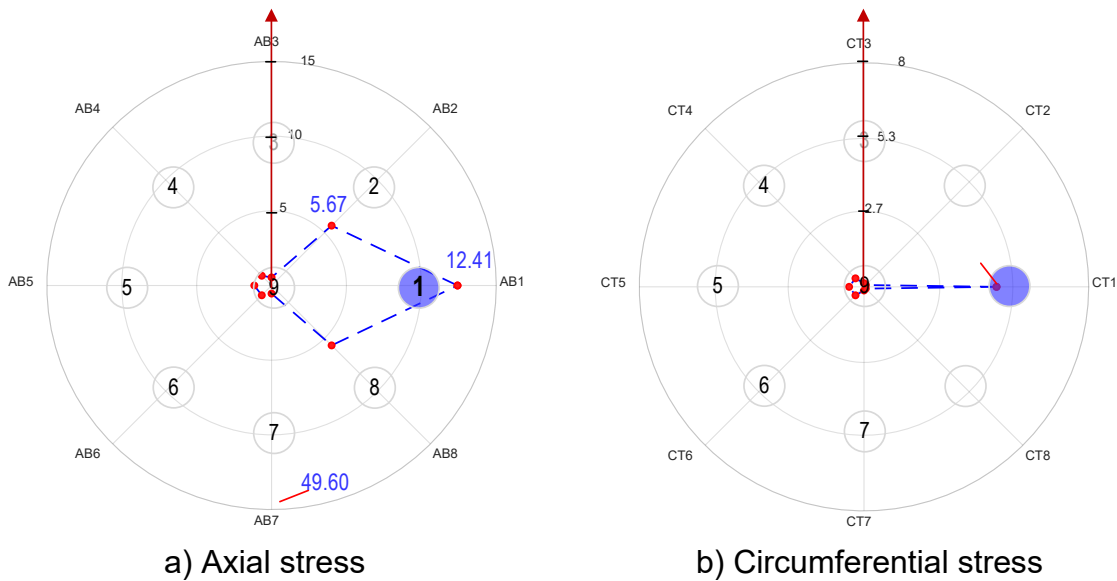
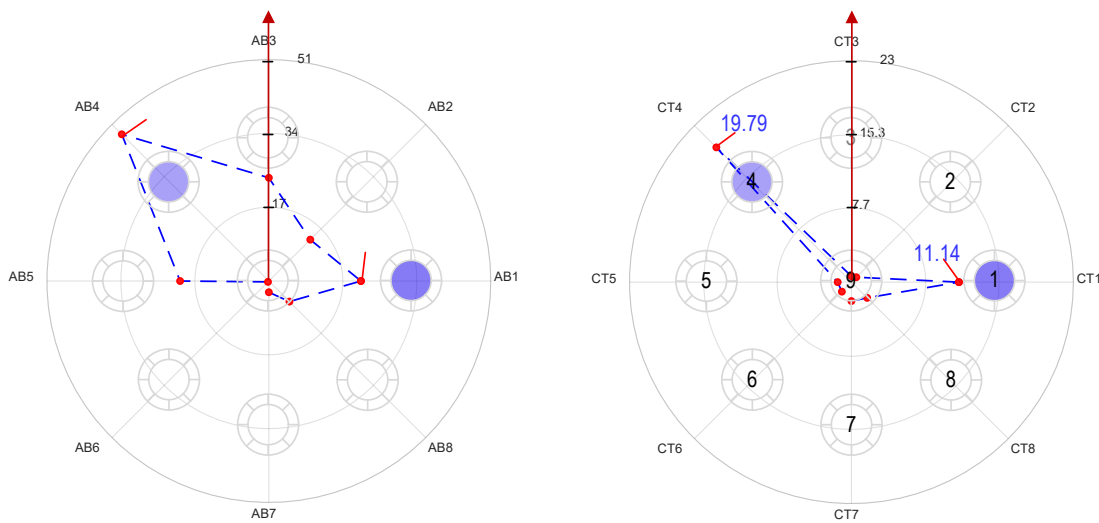


Fig. 6 Numerical stress variations (MPa) under 35 kN loss of Strand 1

The numerical stress variations from Fig. 6 and Fig. 7 reveal that the variation of circumferential stress yields a better indication of the location of damaged strands than that of axial stress.



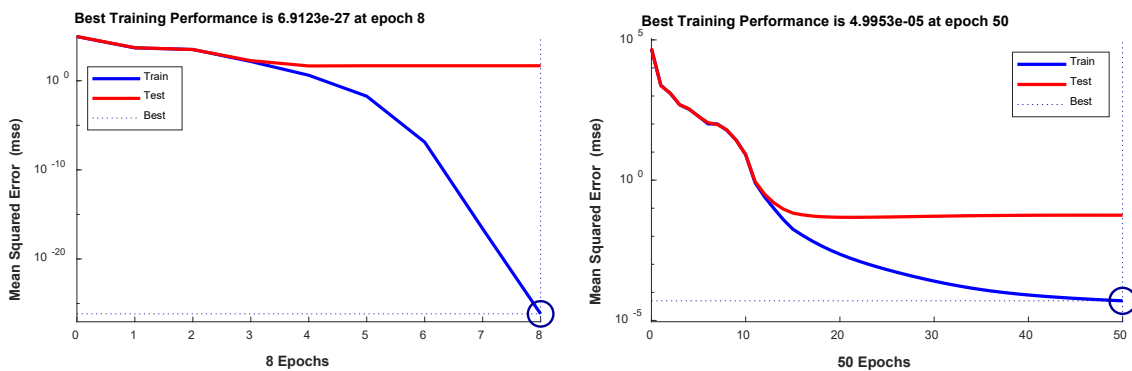
a) Axial stress

b) Circumferential stress

Fig. 7 Numerical stress variations (MPa) under 50 kN force loss of Strand 1 and 70 kN force loss of Strand 4

#### 4. STRAND BREAKAGE DETECTION USING STRESS VARIATION-BASED ANN

Fig. 8a-b shows the training process of the stress variation-based ANN models for prestressing force estimation for AAS and CAM models. For the AAS model, after eight training epochs, the mean squared error reached less than  $10^{-10}$  (see Fig. 8a). For the CAM model, after fifty training epochs, the mean squared error reached less than  $10^{-5}$  (see Fig. 8b).



a) Training AAS model

b) Training CAM

Fig. 8 Training process of variations of stress components-based ANN model

#### 4.1 Identification of Single Damaged Strand

##### Detection of single damaged strand using AAS

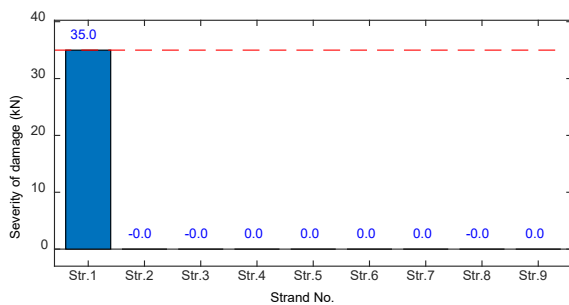
Five simulated damage cases (S1-S5) were selected to demonstrate the performance of single damage detection via the AAS, as listed in Table 2. It is noted that

the force losses in cases S1-S2 belong to training patterns while the force losses in cases S1-S5 were un-training patterns. The estimation of force loss using the AAS model for five simulated cases was also listed in Table 2. As seen in the table, the difference between the inflicted force loss and the estimation at the damaged strand was relatively small (less than 2%, except for case S5).

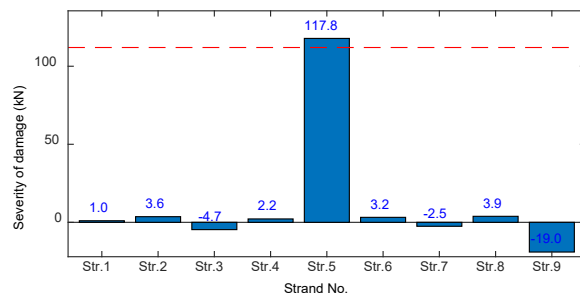
Fig. 8a-c shows the prediction of damaged strand location and the estimation of force loss using the AAS model for the damage cases of Strand 1 (training pattern), Strand 5 (un-training pattern), and Strand 9 (training pattern), respectively. The locations of the damaged strand were accurately localized. There exists a small error for the prediction of Strand 5 damaged in damage case S5 (see Fig. 8b).

Table 2 Simulated single damaged strand in prestressed anchorage

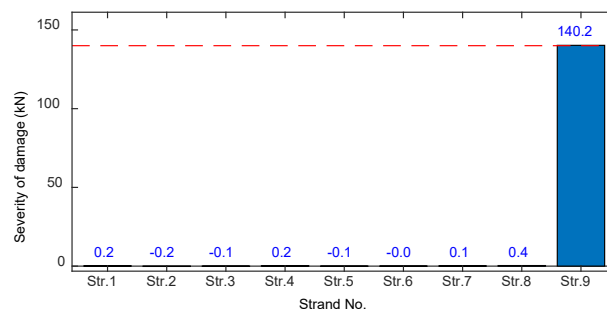
| Case                      | Training patterns |        | Un-Training patterns |       |        |
|---------------------------|-------------------|--------|----------------------|-------|--------|
|                           | S1                | S2     | S3                   | S4    | S5     |
| Damaged strand            | 1                 | 9      | 2                    | 3     | 5      |
| Simulated force loss (kN) | 35                | 140    | 56                   | 84    | 112    |
| Estimation using AAS      | 35.0              | 140.22 | 56.5                 | 82.5  | 117.8  |
| Differences (%)           | 0.0%              | -0.2%  | -0.9%                | 1.9%  | -4.9%  |
| Estimation using CAS      | 35.0              | 143.43 | 56.49                | 82.79 | 124.73 |
| Differences (%)           | 0.0%              | -2.4%  | -0.9%                | 1.5%  | -10.2% |



a) Damaged Strand 1 (S1)



b) Damaged Strand 5 (S5)



c) Damaged Strand 9 (S2)

Fig. 9 Estimation of prestressing force loss using AAS model for single damage case

Detection of single damaged strand using CAS

Five simulated damage cases (S1-S5) were also selected to demonstrate the performance of single damage detection via the CAS, as listed in Table 2. The estimation of force loss using the CAS model for five simulated cases was also listed in Table 2. Fig. 10a-c shows the prediction of damaged strand location and the estimation of force loss using the CAS model for the damage cases of Strand 1 (training pattern), Strand 5 (un-training pattern), and Strand 9 (training pattern), respectively. The locations of the damaged strand were accurately localized. There exists a small error for the prediction of Strand 5 damaged in damage case S5 in the training pattern, as seen in Fig. 10b.

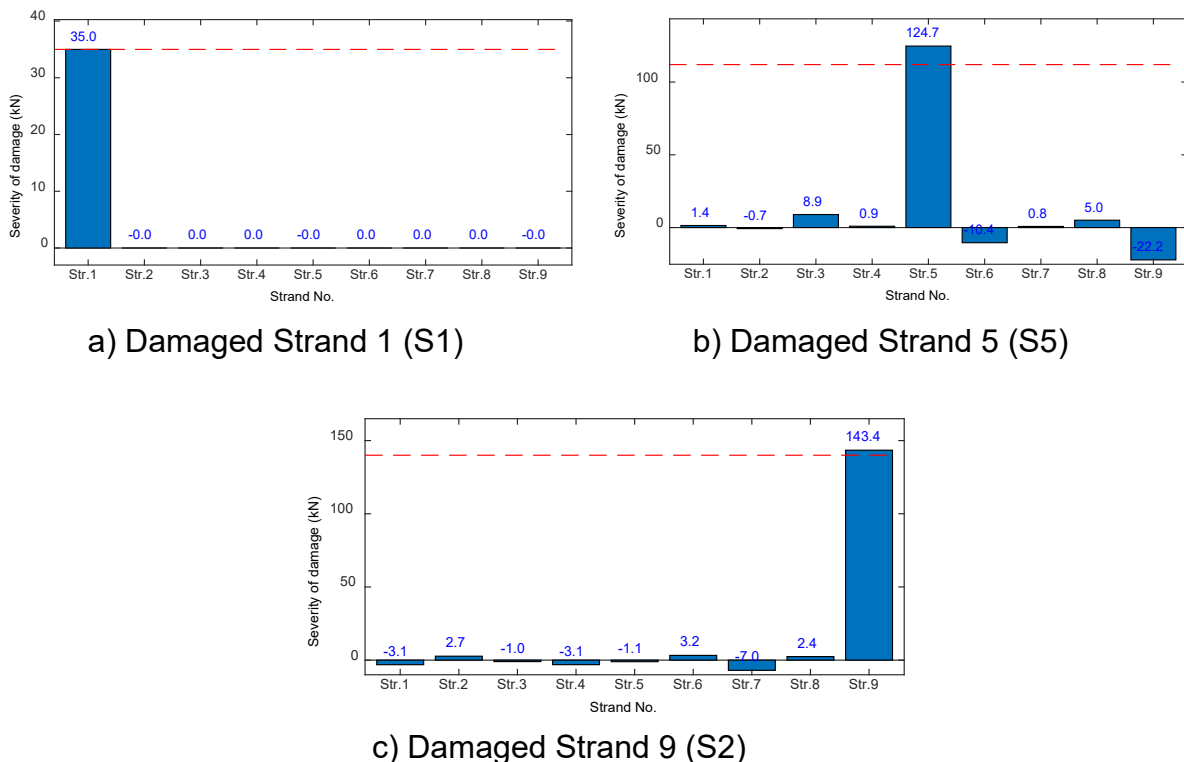


Fig. 10 Estimation of prestressing force loss using CAS model for single damage case

4.2 Identification of Multiple Damaged Strands

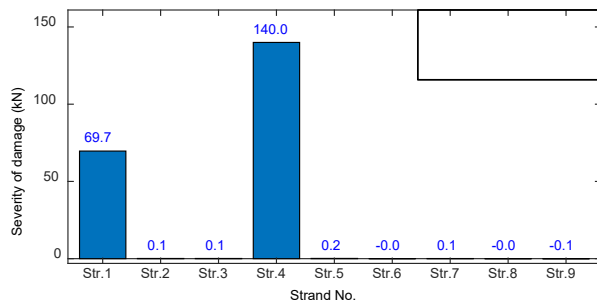
Detection of multiple damaged strands using the AAM

Five simulated damage cases (M1-M5) were selected to demonstrate the performance of single damage detection via the AAM, as listed in Table 3. Two prestressing strands were randomly selected to reduce prestressing force in each simulated case. The estimation of force loss at two damaged strands using the AAM model for five simulated cases was also listed in Table 3. As seen in the table, the difference between the inflicted force loss and the estimation was relatively small (less than 1%).

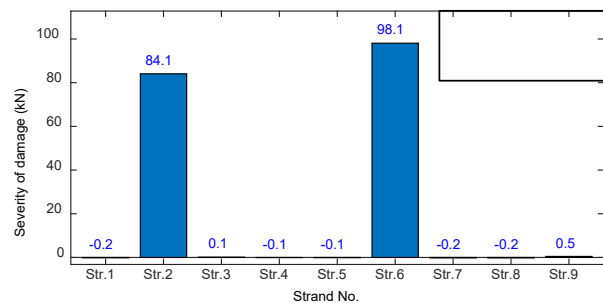
Fig. 11a-c shows the prediction of damaged strand locations and the estimation of force losses using the AAM model for the damage cases M3, M4, and M5, respectively. The locations of the damaged strand were accurately localized.

Table 3 Simulation of multiple damaged strands in prestressed anchorage

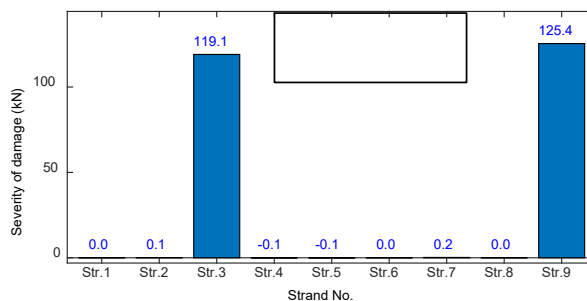
| Case                      | M1   |       | M2    |       | M3    |       | M4    |       | M5    |       |
|---------------------------|------|-------|-------|-------|-------|-------|-------|-------|-------|-------|
| Damaged strands           | 1    | 2     | 1     | 3     | 1     | 4     | 2     | 6     | 3     | 9     |
| Simulated force loss (kN) | 70   | 70    | 70    | 140   | 56    | 140   | 84    | 98    | 119   | 126   |
| Estimated force using AAM | 69.8 | 70.0  | 69.7  | 140.0 | 56.4  | 70.3  | 84.1  | 98.1  | 119.1 | 125.4 |
| Differences (%)           | 0.3% | 0.0%  | 0.5%  | 0.0%  | -0.6% | -0.4% | -0.1% | -0.1% | -0.1% | 0.4%  |
| Estimated force using CAM | 70.0 | 70.1  | 70.1  | 140.0 | 56.0  | 70.1  | 84.1  | 98.1  | 119.0 | 126.0 |
| Differences (%)           | 0.0% | -0.1% | -0.1% | 0.0%  | 0.1%  | -0.1% | -0.1% | -0.1% | 0.0%  | 0.0%  |



a) Damaged Strands 1&4 (M3)



b) Damaged Strands 2&6 (M4)



c) Damaged Strands 3&9 (M5)

Fig. 11 Estimation of force losses using AAM model for multiple damage cases

Detection of multiple damaged strands using CAM

Five simulated damage cases (M1-M5) were selected to demonstrate the performance of single damage detection via the CAM, as listed in Table 3. Two prestressing strands were randomly selected to reduce prestressing force in each simulated case. The estimation of force loss at two damaged strands using the CAM model for five simulated cases was also listed in Table 3. As seen in the table, the difference between the inflicted force loss and the estimation was relatively small (less than 1 %).

Fig. 12a-c show the prediction of damaged strand locations and the estimation of force losses using the CAM model for the damage cases M3, M4, and M5, respectively. The locations of the damaged strand were accurately localized.

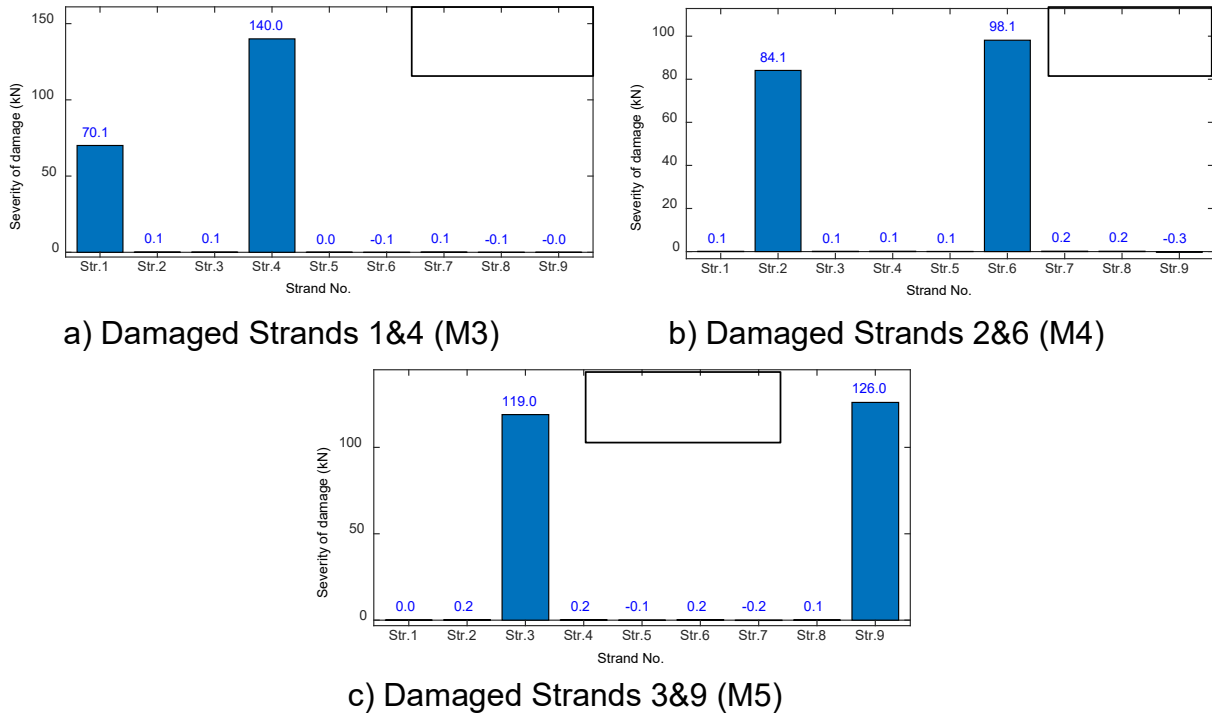


Fig. 12 Estimation of force losses using CAM model for multiple damage cases

## 5. EXPERIMENTAL EVALUATION OF TRAINED ANN-BASED STRAND BREAKAGE DETECTION

### 5.1 Design of Test Structure and Sensor Deployment

#### Experimental Set-up

A supported steel frame was designed to resist tension in prestressed strands of the multi-strand anchorage (Dang *et al.* 2020). The frame consists of the left plate (i.e., a dead-end), the right plate (i.e., a live-end), and four columns connecting to the plates using bolts. The strands anchored on the dead-end by the anchor head were distributed and passed through into multiple holes on the live end. Load cells installed at the right ends of strands were used to measure actual forces in the prestressed strands.

A multi-strands anchorage comprises a 9-strands anchor head with wedges and a bearing plate, as shown in Fig. 13. The designed geometry of the anchorage was based on the post-tensioning system (Type E anchorage). The bearing plate had a size of 270×270×45 mm, the anchor head had a diameter of 159 mm and 65 mm in height, and the wedges had the bottom and top diameters of 29 mm and 17 mm, respectively. The material properties of the steel anchorage components are defined as follows:  $E = 200$  GPa (Young modulus),  $\nu = 0.33$  (Poisson ratio), and  $\rho = 7850$  kg/m<sup>3</sup> (mass density).

The prestressed strands (see Fig. 13c) that have 15.2 mm in diameter were comprised of seven wires. The strands were designed with  $E = 195 \text{ GPa}$ , a tensile strength of 260 kN. The left ends of the strands were gripped onto conical holes in the anchor head by three-piece cone wedges. The right ends of the strands were designed with threads connecting to hydraulic jacks to control the prestress forces.

To measure strain responses of the multi-strands anchorage, 12 ESGs were deployed at the near-top and near-bottom anchor head, as shown in (see Fig. 13a-b). Specifically, six ESGs (namely CT1-CT3 and CT6-CT8) were positioned at the near-top anchor head to measure circumferential stress. The ESGs were placed about 3mm from the top of a surface plate of the anchor head. Six ESGs (namely CB 1-3 and CB 6-8) were positioned at the near-bottom anchor head to capture axial strains of the anchor head, and they was placed about 5 mm from the bearing plate's surface. The signal conditioner for strain measurement consists of bridge boxes, a data recorder, and a laptop for operations. The sampling frequency was set as 1 Hz, and the measurement time was set as 25 seconds.

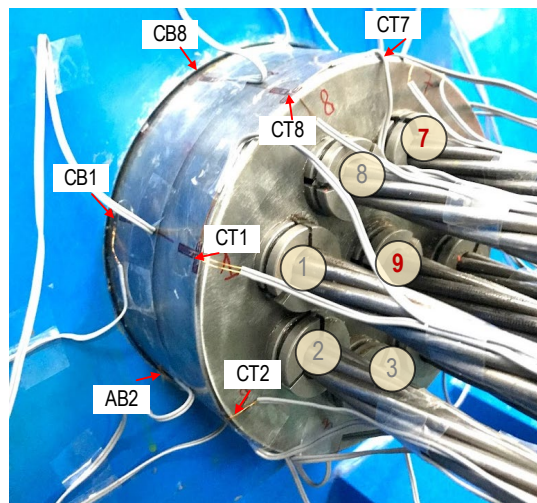
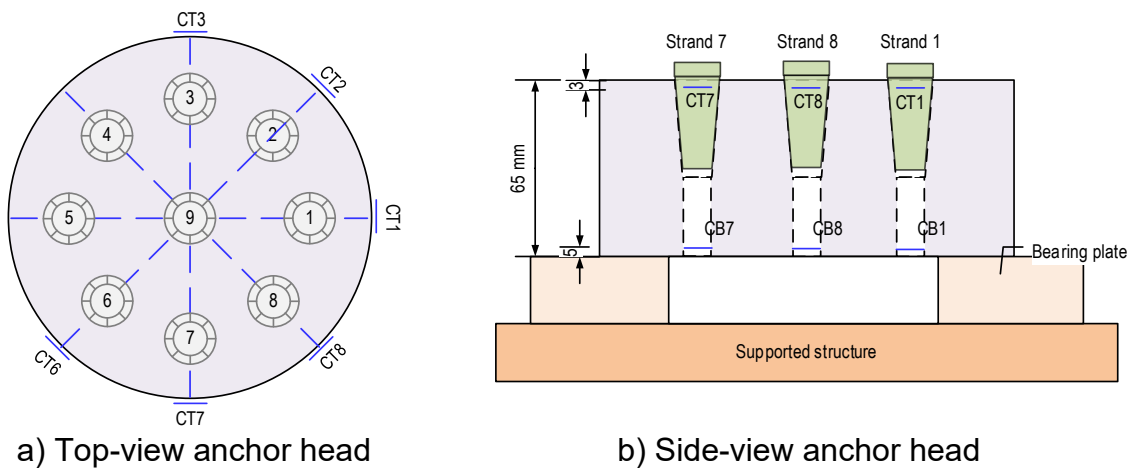


Fig. 13 Design of multi-strand system and ESGs deployment (dimension in mm)

Simulated cases of prestress loss for strain measurement

Four test cases (TC1-TC4) were designed for the full-scale anchorage, as listed in Table 4. The test cases TC1 and TC3 were designed as intact cases. Meanwhile, the test cases TC2 and TC4 were simulated for the damage cases corresponding to the breakages of Strand 7 and Strand 9. Specifically, firstly, all nine strands were stressed up to an average tension of approximately 138.2 kN to simulate the intact case TC1. Next, the prestress force of Strand 7 was reduced to 69.9 kN keeping near-constant force in other strands to simulate the damaged Strand 7. Then, Strand 7 was re-pulled to approximately 136.4 kN to simulate the intact case TC3. Finally, the prestress force of Strand 9 was reduced to simulate the damaged Strand 4 in the test case TC4. As shown in Table 4, the breakage of a single strand caused slight changes in the prestress forces of the remaining strands.

Table 4 Simulation cases of strand breakage for strain measurements

| Case                      | Actual prestress forces (kN) |        |        |        |        |        |             |        |             |
|---------------------------|------------------------------|--------|--------|--------|--------|--------|-------------|--------|-------------|
|                           | Str. 1                       | Str. 2 | Str. 3 | Str. 4 | Str. 5 | Str. 6 | Str. 7      | Str. 8 | Str. 9      |
| TC1<br>(Intact 1)         | 139.3                        | 137.1  | 139.3  | 136.2  | 136.8  | 137.7  | 139.8       | 139.3  | 141.3       |
| TC2<br>(loss of Strand 7) | 139.5                        | 137.3  | 140.3  | 136.9  | 137.9  | 139.1  | <b>69.9</b> | 139.1  | 139.3       |
| TC3<br>(Intact 2)         | 138.5                        | 136.6  | 139.3  | 136.0  | 136.6  | 137.5  | 136.4       | 137.7  | 139.3       |
| TC4<br>(Loss of Strand 9) | 139.3                        | 137.3  | 140.3  | 137.1  | 137.3  | 138.5  | 137.3       | 138.9  | <b>69.7</b> |

5.2 Experimental Stress Responses of Multi-strands Anchorage

Measured strain variations

The strain responses of the multi-strands anchorage were recorded for all testing cases (TC1-TC4). Due to the symmetry of the anchorage (see Fig. 13c), it is assumed that the strain components at Strand 4 and Strand 5 are the same as those at Strand 2 and Strand 1, respectively.

As listed in Table 5, the strain variations were computed for the axial strain. It is noted from the tables that the negative strain variation indicates more compression, while the positive value indicates more tension. As seen in the table, the damage of the outer Strand 7 caused a significant strain change at locations close to the damaged strands (i.e., AB7 or AB6). Meanwhile, the damage to center Strand 9 caused near-stress changes for all measured strain sensors.

As listed in Table 6, the strain variations were computed for the circumferential strain. As seen in the table, the damage of the outer Strand 7 caused a significant circumferential strain change at Strand 7 (i.e., AB7), while changes in others were ignorable. The damage of center Strand 9 caused near-stress changes for all measured strain sensors.

Table 5 Variations of axial strain ( $\mu\epsilon$ ) at near-bottom anchor head

| Sensor           | AB 1  | AB 2   | AB 3   | AB4    | AB5   | AB 6  | AB 7   | AB 8  |
|------------------|-------|--------|--------|--------|-------|-------|--------|-------|
| Damaged Strand 7 | 6.17  | -11.76 | -17.05 | -11.76 | 6.17  | 49.24 | 126.08 | 52.25 |
| Damaged Strand 9 | 12.77 | 12.71  | 18.97  | 15.06  | 12.77 | 12.71 | 18.97  | 15.06 |

Table 6 Variations of circumferential strain ( $\mu\epsilon$ ) at near-top anchor head

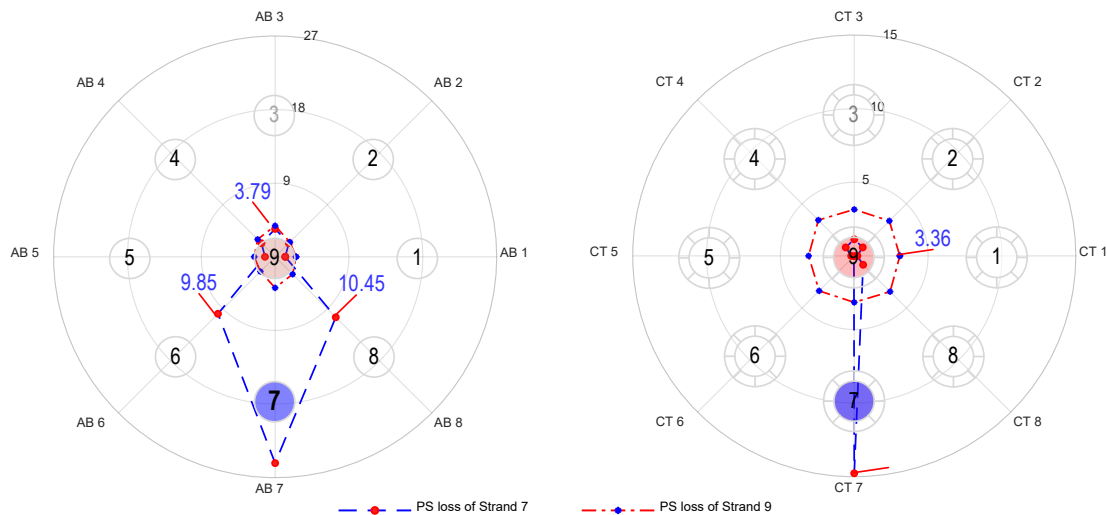
| Sensor           | CB 1  | CB 2  | CB 3  | CB4   | CB5   | CB 6  | CB 7  | CB 8  |
|------------------|-------|-------|-------|-------|-------|-------|-------|-------|
| Damaged Strand 7 | 1.02  | 4.06  | 5.65  | 4.06  | 1.02  | -0.15 | 73.81 | 4.26  |
| Damaged Strand 9 | 15.44 | 16.80 | 15.77 | 17.17 | 15.44 | 16.80 | 15.77 | 17.17 |

### Experimental Stress Variation

By assuming that the stress-strain relationship follows Hooke's law, the stress variation in the anchorage was computed as follows:

$$\Delta\sigma_p = E\Delta\epsilon_p \quad (1)$$

where  $\Delta\sigma_p$  signifies the stress variation,  $E$  is the Young modulus of the anchorage ( $E = 200$  GPa), and  $\Delta\epsilon_p$  is the strain change after and before damaged strands.



a) Axial stress (near-bottom)      b) Circumferential stress (near-top)  
 Fig. 14 Experimental stress variation (MPa) induced by Strand 7 damaged and Strand 9 damaged

The variation of the axial stress in the anchor head was plotted over the cross-section under the damaged Strands 7 and 9, as shown in Fig. 14a. It is observed that the

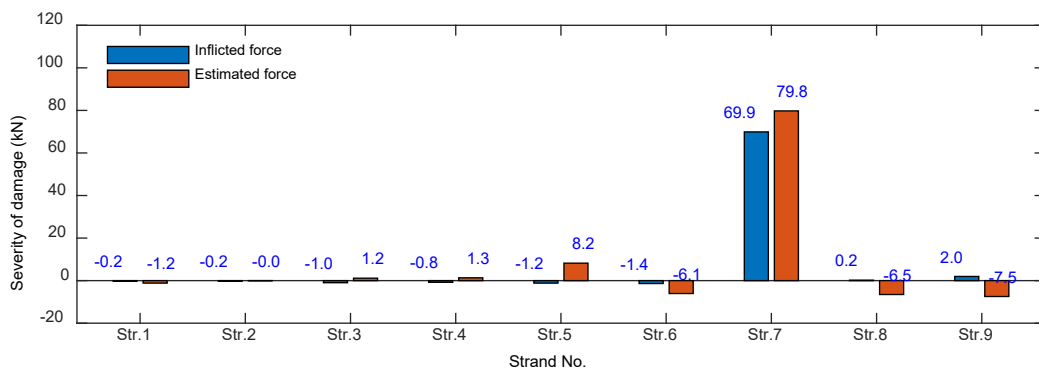
breakage of the outer Strand 7 caused significant changes in the axial stresses at the locations close to Strand 7. Meanwhile, the breakage of the center Strand 9 caused almost equal stress variations.

The variation of the circumferential stress was plotted over the cross-section of the anchor head under the damaged Strands 7 and 9, as shown in Fig. 14a. The breakage of the outer strand caused significant stress changes at the locations close to the damaged strand, while the breakage of the center strand caused relatively uniform stress variations. This observation was consistent with numerical stress variation result (See Section 3).

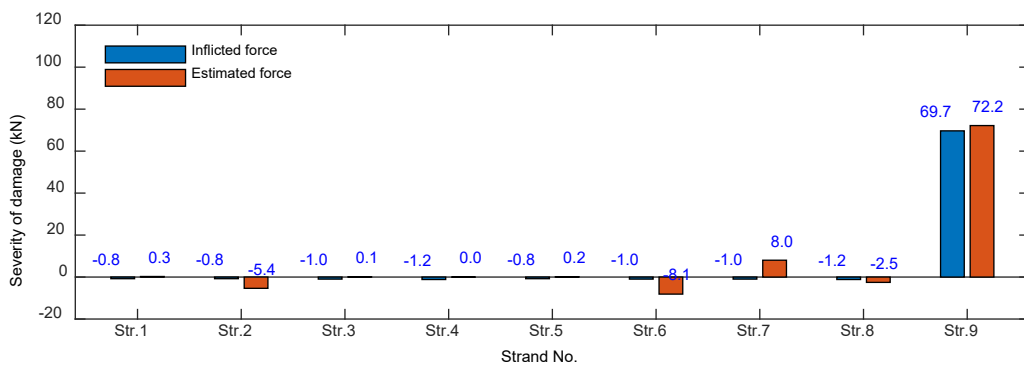
### 5.3 Detection of damaged strand using trained ANN models

#### Experimental estimation of stress variation using AAS model

To evaluate the accuracy of the ANN model for force loss estimation, the axial stress variation, calculated from the measured strain (see Table 5), was input to the AAS model to estimate force losses. Fig. 15a-b shows a comparison between the variations of inflicting force and the estimated one for two damage cases of outer Strand 7 and center Strand 9. It is noted that the inflicted force was the difference of force before and after strand breakage (see Table 4).



a) Damage of Strand 7



b) Damage of Strand 9

Fig. 15 Estimation of stress variation (MPa) using AAS model for strand breakage

As seen in the figures, the predicted force at the damaged strand was the most significant, and the ones at other strands were insignificant. Specifically, for the breakage

of Strand 7 (see Fig. 15a), the predicted force loss (79.8 kN) was about 10% difference compared with the simulated one (69.9 kN). For the breakage of Strand 9 (see Fig. 15b), the predicted force loss (72.2 kN) shows a good agreement with the simulated one (69.7 kN).

Experimental estimation of stress variation using CAS model

To evaluate the accuracy of the CAS model for force loss estimation, the circumferential stress variation, extracted from the measured strain (see Table 6), was input to the CAS model to estimate force losses. Fig. 16a-b shows a comparison between the variations of inflicting force and the estimated one for two damage cases of outer Strand 7 and center Strand 9. The predicted force at the damaged strand was the most significant, and the ones at other strands were insignificant. Specifically, for the breakage of Strand 7 (Fig. 16a), the predicted force loss (107.4 kN) was about 1.5 times larger than the simulated one (69.9 kN). For the breakage of Strand 9 (Fig. 16b), the predicted force loss (85.1 kN) was about 20% larger than the inflicted one (69.7 kN).

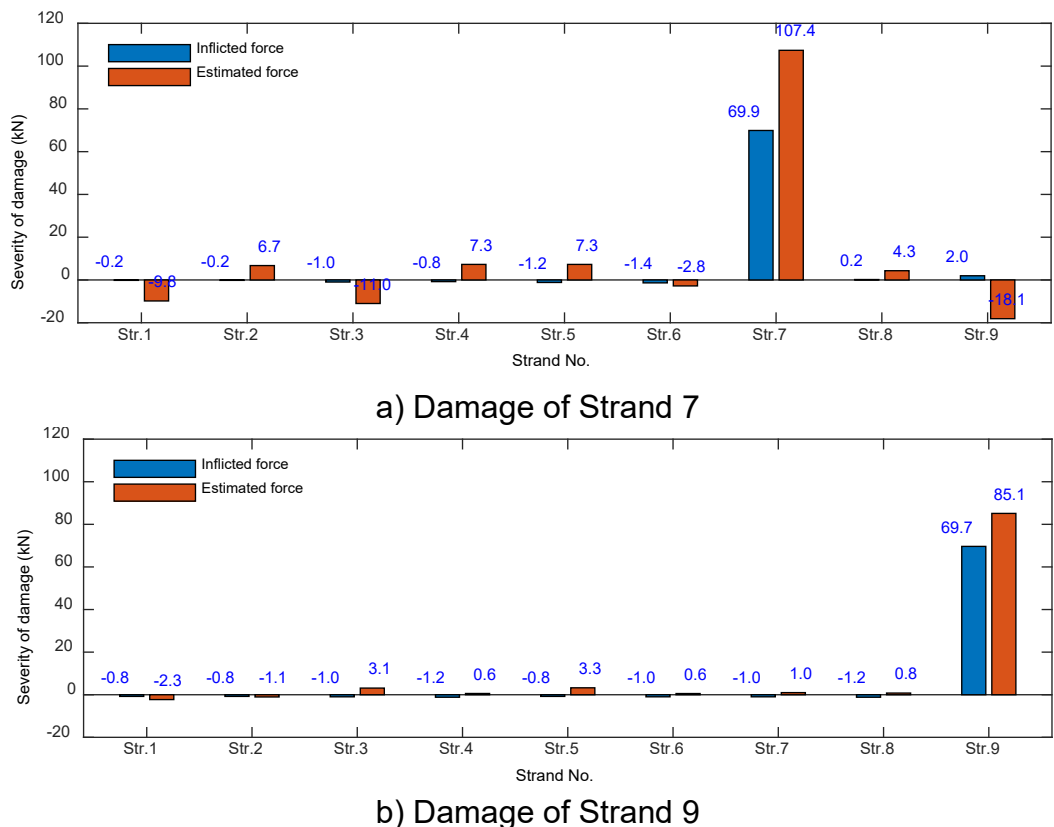


Fig. 16 Estimation of stress variation (MPa) using CAS model for strand breakage

**6. CONCLUDING REMARKS**

This study presented strand breakage identification in a prestressed anchorage using stress variation-based ANN algorithm. Firstly, a scheme of stress variation-based ANN was designed for damage detection in the anchorage structures. Secondly, the FE model of the multi-strand anchorage was analyzed to generate training patterns under

various single and multiple damaged strand cases. Third, the ANN algorithms were employed to detect damaged strand locations and severities in the multi-strand anchorage. Last, the feasibility of trained ANN models for prestress loss estimation was tested using experimental data.

From numerical and experimental evaluation, the following conclusion can be drawn. First, the feasibility evaluation of the stress variation-based ANN model for strand breakage identification was successfully tested. Second, circumferential stress changes, measured at the near-top anchor, show a better indication for both single and multiple damages. Third, prestress loss estimation using experimental axial-stress changes-based ANN yielded better accuracy than that using circumferential ones. Last, the circumferential stress at the near-top anchor and axial measured at the near-bottom anchor should be concurrently utilized for localizing damaged strands and estimating prestress loss.

### **ACKNOWLEDGMENT**

This research was supported by a grant (21CTAP-C163708-01) from the Technology Advancement Research Program funded by Korea Agency for Infrastructure Technology Advancement (KAIA). The graduate student was also supported by the 4<sup>th</sup> BK21 program of Korean Government.

### **REFERENCE**

- Abdullah, A. B. M., Rice, J. A. and Hamilton, H. R. (2015a), "Wire breakage detection using relative strain variation in unbonded posttensioning anchors", *Journal of Bridge Engineering*, Vol. **20** (1), pp. 1-12.
- Abdullah, A. B. M., Rice, J. A. and Hamilton, H. R. (2015b), "A strain-based wire breakage identification algorithm for unbonded PT tendons", *Smart Structures and Systems*, Vol. **16** (3), pp. 415-433.
- Barr, P. J., Kukay, B. M. and Halling, M. W. (2008), "Comparison of prestress losses for a prestress concrete bridge made with high-performance concrete", *Journal of Bridge Engineering*, Vol. **13** (5), pp. 468-475.
- Chen, H. L. and Wissawapaisal, K. (2001), "Measurement of tensile forces in a seven-wire prestressing strand using stress waves", *Journal of Engineering Mechanics*, Vol. **127** (6), pp. 599-606.
- Dang, N. L., Huynh, T. C. and Kim, J. T. (2019), "Local strand-breakage detection in multi-strand anchorage system using an impedance-based stress monitoring method-feasibility study", *Sensors (Basel)*, Vol. **19** (5).
- Dang, N. L., Huynh, T. C., Pham, Q. Q., Lee, S. Y. and Kim, J. T. (2020), "Damage-sensitive impedance sensor placement on multi-strand anchorage based on local stress variation analysis", *Structural Control and Health Monitoring*, Vol. **27**, pp. e2547.
- Hamed, E. and Frostig, Y. (2006), "Natural frequencies of bonded and unbonded prestressed beams—prestressing force effects", *Journal of Sound and Vibration*, Vol. **295** (1-2), pp. 28-39.
- Ho, D. D., Kim, J. T., Stubbs, N. and Park, W. S. (2012), "Prestress-force estimation in PSC girder using modal parameters and system identification", *Advances in Structural Engineering*, Vol. **15** (6), pp. 997-1012.
- Huynh, T. C. and Kim, J. T. (2014), "Impedance-based cable force monitoring in tendon-anchorage using portable PZT-interface technique", *Mathematical Problems in Engineering*, Vol. **2014**, pp. 1-11.

- Huynh, T. C., Park, Y. H., Park, J. H. and Kim, J. T. (2015), "Feasibility verification of mountable PZT-interface for impedance monitoring in tendon-anchorage", *Shock and Vibration*, Vol. **2015**, pp. 1-11.
- Huynh, T. C. and Kim, J. T. (2017), "Quantification of temperature effect on impedance monitoring via PZT interface for prestressed tendon anchorage", *Smart Materials and Structures*, Vol. **26 (12)**, pp. 1-19.
- Kim, J. T., Yun, C. B., Ryu, Y. S. and Cho, H. M. (2004), "Identification of prestress-loss in PSC beams using modal information", *Structural Engineering and Mechanics*, Vol. **17 (3\_4)**, pp. 467-482.
- Kim, J. T., Park, J. H., Hong, D. S. and Park, W. S. (2010), "Hybrid health monitoring of prestressed concrete girder bridges by sequential vibration-impedance approaches", *Engineering Structures*, Vol. **32 (1)**, pp. 115-128.
- Law, S. S. and Lu, Z. R. (2005), "Time domain responses of a prestressed beam and prestress identification", *Journal of Sound and Vibration*, Vol. **288 (4-5)**, pp. 1011-1025.
- Min, J., Yun, C. B. and Hong, J. W. (2016), "An electromechanical impedance-based method for tensile force estimation and damage diagnosis of post-tensioning systems", *Smart Structures and Systems*, Vol. **17 (1)**, pp. 107-122.
- Salamone, S., Bartoli, I., Phillips, R., Nucera, C. and Di Scalea, F. (2011), "Health Monitoring of Prestressing Tendons in Posttensioned Concrete Bridges", *Transportation Research Record: Journal of the Transportation Research Board*, Vol. **2220**, pp. 21-27.
- Spencer, B. F., Hoskere, V. and Narazaki, Y. (2019), "Advances in computer vision-based civil infrastructure inspection and monitoring", *Engineering*, Vol. **5 (2)**, pp. 199-222.
- Tadros, M. K., Omaishin, N. A., Seguirant, S. J. and Gallt, J. G. (2003), *Prestress losses in pretensioned high-strength concrete bridge girders*. Transportation Research Board.
- Zhang, X., Zhou, W. and Li, H. (2019), "Electromechanical impedance-based ice detection of stay cables with temperature compensation", *Structural Control and Health Monitoring*, Vol. **26 (9)**.
- Zui, H., Shinke, T. and Namita, Y. (1996), "Practical formulas for estimation of cable tension by vibration method", *Journal of Structural Engineering*, Vol. **122 (6)**, pp. 651-656.